J Solid State Electrochem (2010) 14:1541–1546
DOI 10.1007/s10008-009-0982-3

ORIGINAL PAPER

Fabrication of double-walled carbon nanotube counter electrodes for dye-sensitized solar sells

D. W. Zhang · X. D. Li · S. Chen · F. Tao · Z. Sun · X. J. Yin · S. M. Huang

Received: 11 September 2009 / Revised: 17 November 2009 / Accepted: 18 November 2009 / Published online: 3 December 2009

Abstract Double-walled carbon nanotubes (DWCNTs) have been studied for counter-electrode application in dye-sensitized solar cells (DSCs). Mesoporous TiO2 films are prepared from the commercial TiO2 nanopowders by screen-printing technique on optically transparent-conducting glasses. A metal-free organic dye (indoline dye D102) is used as a sensitizer. DWCNTs are applied to substitute for platinum as counter-electrode materials. Morphological and electrochemical properties of the formed counter electrodes are investigated by scanning electronic microscopy and electrochemical impedance spectroscopy, respectively. The electronic and ionic processes in platinum and DWCNT-based DSCs are analyzed and discussed. The catalytic activity and DSC performance of DWCNTs and Pt are compared. A conversion efficiency of 6.07% has been obtained for DWCNT counter-electrode DSCs. This efficiency is comparable to that of platinum counter-electrode-based devices.

Keywords Dye-sensitized solar cell · Nanocrystallined TiO2 · Metal-free organic dye · Counter electrode · Double-walled carbon nanotube (DWCNT)

D. W. Zhang · X. D. Li · S. Chen · F. Tao · Z. Sun · S. M. Huang (✉)
Engineering Research Center for Nanophotonics & Advanced Instrument, Ministry of Education, Department of Physics, East China Normal University,
North Zhongshan Rd. 3663,
Shanghai 200062, People's Republic of China
e-mail: smhuang@phy.ecnu.edu.cn

X. J. Yin
Advanced Materials Technology Centre, Singapore Polytechnic,
500 Dover Rd.,
Singapore 139651, Singapore

Introduction

Dye-sensitized solar cells (DSCs) have been studied intensively due to their advantages in economic, scientific, and technical aspects since their conversion efficiencies exceeded 11% [1–4]. Counter electrode plays a key role in DSC. It helps the regeneration of redox couples in electrolyte and makes the cell a complete circuit. Previous studies have shown that platinum is superior toward tri-iodide reduction in DSCs; however, cost and stability considerations necessitate the development of alternative material [5]. Hence, other materials are attempted to reduce production cost of DSCs. Some carbonaceous materials such as nanosize carbon powders, activated carbon, and graphite have been employed as catalysts for counter electrodes to replace the Pt electrode [6–8]. Catalytic activity toward I_3^- reduction has been observed on these carbon-based counter electrodes, but an overall energy conversion efficiency of the device is below than that of conventional Pt counter-electrode DSCs. Besides, nanocarbon counter electrode poses additional risk to the stability of DSCs. Since the electrodes made up of nanosize carbon powder, prolonged exposure in corrosive I^-/I_3^- redox electrolyte may lead to the detachment of loosely bounded particles from rest of the electrode, promoting the dark current and degrading the overall device performance [9].

Due to the high longitudinal conductivity, heat resistance, as well as corrosion resistance and electrocatalytic activity for tri-iodide $\left(I_3^-\right)$ reduction of carbon nanotubes (CNTs), CNTs were thought to have some possibility to replace platinum in the DSC and tested as counter electrodes of the DSCs [10–13]. These materials have several advantages over platinum. Platinum was found to degrade over time while in contact with an iodide/triiodide liquid electrolyte, reducing the efficiency of a DSC, whereas

CNTs did not degrade [10]. Suzuki et al. [10] used single-wall CNTs (SWCNTs) on the fluorine-doped tin oxide (FTO) glass as the counter electrode, achieving a conversion efficiency of 3.5%. Lee et al. [11] applied multi-wall CNTs (MWCNTs) as counter electrodes, demonstrating a conversion efficiency of 3.06%. In particular, Ramasamy et al. [12] applied MWCNT films sprayed on FTO as the counter electrode for DSC. The device exhibited high performance with the energy conversion efficiency (η) of 7.59%, short-circuit current (Jsc) of 15.64 mA cm−2, open-circuit voltage (Voc) of 0.783 V, and fill factor (FF) of 0.62, under a 1,000-W Xe arc lamp. The DSC efficiency was raised to 7.7% by ball milling pretreatment of MWCNTs [13]. Double-walled CNT (DWCNT) is one of the important members of CNT family. As an intermediate state between SWCNT and MWCNT, DWCNT is predicted to have better physical and chemical properties than SWCNT and MWCNT [14–16]. For example, DWCNT has much longer lifetime than SWCNT [16]. Chemical functionalization on the surface of DWCNT can yield exciting and important CNT-based materials while maintaining the properties of the inner tube intact. However, DWCNT is s less exploited material because it involves much more critical synthesis conditions than MWCNT and SWCNT. Nevertheless, synthesis of DWCNTs has been achieved recently [17, 18]. Thus, DWCNTs are going to be widely applied to investigate all kinds of photoelectric devices in the near future due to their unique electric and chemical properties. Good catalytic performance could be expected from DWCNTs as the counter electrodes for DSCs. Following our previous works focused on applying various nanocarbon and CNT thin films to develop negative electrodes for field emission displays (FEDs), flat field emission lamps, and water purification systems [19–22], we explored and developed applications of DWCNTs in DSCs as counter electrodes in this work. Mesoporous TiO2 films were processed from the commercial TiO2 nanopowders by screen-printing technique. DWCNTs were deposited on FTO substrates as counter electrodes. The internal resistance of Pt and DWCNTs counter-electrode-based DSCs were investigated through electrochemical impedance spectroscopy (EIS) measurement. Efficient DSCs using DWCNTs as counter electrodes were fabricated. Their efficiency was very close to that of platinum counter-electrode-based devices.

Experimental

Preparation of counter electrode and characterization

Platinized counter electrodes were printed using a paste based on H2PtCl6 dispersed in a mixture of terpineol and ethylcellulose. The printed layers were heated at 385 °C for 20 min [23]. DWCNT counter electrodes were prepared by a similar way. The DWCNTs (Shenzhen Nanotach Port Co., Ltd., Diameter<5 nm, length <20 μm, purity >90%, special surface area >450 m^2g^{-1}) were ground in a mixture of terpineol and ethylcellulose. The obtained paste was deposited on the cleaned FTO glass by the screen printing method. Then, the printed DWCNT film was heated at 300 °C for 15 min to maintain good adhesion between the DWCNT layer and the FTO substrate. It was found that if the temperature of the printed DWCNT layer was higher than 400 °C, the terpineol and ethyl cellulose was more completely burned out; however, the DWCNT film was easy to be peeled off from the substrate. Thus, there is trade-off between increasing adhesion and increasing electrical conductivity. Considering this trade-off, the annealing temperature of 300 °C was used for preparing DWCNT counter electrodes.

The prepared counter-electrode layers were characterized by field emission scanning electron microscope (FESEM) (JEOL, JSM-6700F). The thickness of the layers was measured by a profilometer (Dektak 6M).

Photoanode fabrication and characterization

A viscous TiO2 paste was prepared based on a procedure of [4]. Firstly, 1 ml acetic acid (AR, SCRC, China) and 6 g TiO2 (P25, Degussa) powder were mixed in an agate mortar. Secondly, 15 ml deionized water and 30 ml anhydrous ethanol (AR, SCRC, China) were introduced drop by drop into the agate mortar under continuous grinding. Thirdly, the mixture was transferred into a beaker with another 50 ml ethanol. After magnetic stirring and ultrasonication, terpineol (AR, SCRC, China) and ethyl cellulose (200cPas, SCRC, China) in ethanol was then added into the beaker. The weight ratio of ethyl cellulose to terpineol is 5 wt.%. Subsequently, alternating stirring and sonication were carried out to get homogeneous slurry. At last, the slurry was concentrated with a rotary evaporator to remove the ethanol and finalized by thoroughly grinding.

The TiO2 working electrodes were prepared using the above paste on FTO glass by the screen print technology. The glass was previously ultrasonically cleaned in ethanol, acetone, and deionized water, respectively. The FTO substrates were treated with 50 mM TiCl4 aqueous solution at 70 °C for 30 min in order to improve the adhesion and mechanical strength of the nanocrystalline TiO2 layer to the FTO layer [4]. A screen (30 μm in thickness, 200mesh/inch) was used to prepare the TiO2 films. The thickness of the film was controlled by the printing times. The screen-printed layer was dried in air at room temperature for 15 min and then kept at 100 °C for 10 min. Then, the film was fired at 500 °C in air for 30 min.

A metal-free organic dye (indoline dye D102) [24, 25] was used as a sensitizer. The D102 dye was purchased from Shanghai Green-Technology Co., Ltd. The dye was of high purity (≥98%) and high absorption coefficient (67,500 L $mol^{-1}cm^{-1}$ at 501 nm). After sintering at 500 °C and cooling down to 80 °C, the nanostructured TiO2 films were immersed into the dye solution at room temperature for 15 h. The sensitizing dye solution contained 0.5 mM indoline dye D102 in acetonitrile and *tert*-butyl alcohol (volume ratio=1:1). A red color was developed after immersion, indicating that chemisorption took place and confirmed the dye grafting on the semiconductor surface. The TiO2 electrodes were then rinsed with absolute ethanol to eliminate the physisorbed dye, dried in air, and ready for the next step use.

A cell holder equipped with clamps was used to press the TiO2 working electrode and the counter electrode. A drop of electrolyte solution (0.1 M LiI, 0.05 M I2, 0.6 M DMPII, and 0.05 M *tert*-buthylpyridine in 3-methyoxypropionitrile) was introduced into the clamped electrodes. An adhesive tape (approximately 40 μm thick, 3M Scotch) was placed between the photoelectrode and the counter electrode to avoid short-circuiting.

Photoelectrochemical characteristics of the DSCs were analyzed by EIS [26]. The EIS spectra were measured with a computer-controlled electrochemical workstation (CHI660B). EIS of DSC was performed under constant light illumination and open-circuit conditions. The measurement was carried on the AC impedance analyzer from 0.1 Hz to 100 KHz with perturbation amplitude of 10 mV. The photovoltaic performance parameters of DSCs were measured under a simulated illumination (Solar simulator, Newport Oriel 93194A) with a light intensity of 60 mW cm−2. As reported by Grätzel M. in [27], the DSC exhibited the highest overall efficiency with the light intensity of 65 mW cm−2, whereas a slightly lower efficiency value with an intensity of 100 mW $cm^{-}2$. The area of the dye-coated TiO2 electrode was 0.25 cm2.

Results and discussion

Figure 1a and b shows FESEM images of DWCNT and Pt electrodes deposited on FTO glass substrates, respectively. The DWCNTs were twisted and connected to each other to form a three-dimensional (3D) network structure with a thickness of ~7.0 μm as shown in Fig. 1a and b. A few angstrom wide I_3^- ions can easily diffuse into the pores and get reduced, suggesting that DWCNT counter electrode had high electrochemical active surface [28]. Figure 1c and d shows typical SEM images of the platinum film of the

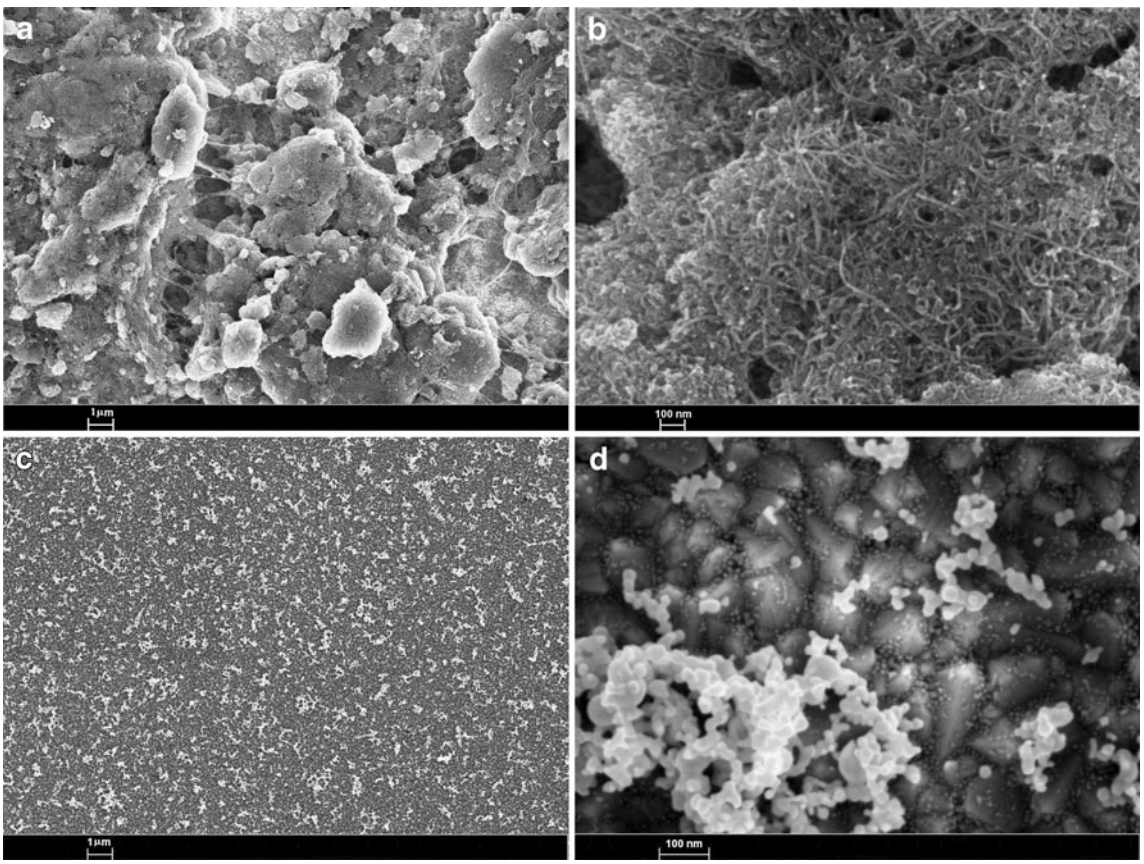

Fig. 1 FESEM images of prepared counter-electrode layers deposited on FTO glass substrates. DWCNT (**a**, **b**), Pt (**c**, **d**)

electrode prepared by thermal decomposition. Uneven size distribution was observed for Pt particles. The irregular and rough crystalline structure under the platinum film due to the fluorine-doped SnO2 layer coated on the glass sheet and the 5–15-nm-sized platinum clusters seemed mainly distributed and aggregated in the gap between SnO2 particles on the surface of FTO, as shown as in a Fig. 1d with a higher magnification. The effect of the thickness of the Pt film on the performance of DSCs was investigated in details by Fang et al. [29]. Their results indicated that when the Pt film thickness exceeded 100 nm, further Pt deposition had no significant influence on improvement in the conductivity, charge-transfer resistance, and the catalytic activity. In our work, the thickness of coated Pt was about 200 nm.

Figure 2 shows photocurrent voltage (*I–V*) curves of DSCs fabricated with DWCNTs and Pt-based counter electrodes, respectively, under a light intensity of 60 mW cm−2. Diode parameters (*J*sc, *V*oc, FF, and η) were measured on multiple devices to obviate cell-to-cell fabrication differences. The average measured diode parameters for DSCs based on both kinds of counter electrodes along with statistics are summarized in Table 1. For all the DSCs made, the thickness of the TiO2 layer was about 10 μm. DSC with DWCNTs as counter electrode showed 6.05% overall light to electric energy conversion efficiency, which was quite comparable to the performance (6.80%) of platinum counter-electrode device, as listed in Table 1.

EIS has been widely used to investigate the interfacial charge transfer processes occurring in DSCs [30–32]. In order to understand the difference in *I–V* performance of DSCs fabricated with DWCNT and Pt counter electrodes, respectively, EIS measurement also carried out under constant light illumination (60 mW cm−2) biased at open-circuit condition. Figure 3 shows the impedance spectra of DSCs fabricated with both kinds of counter electrodes. The

Table 1 Performance characteristics of DSCs fabricated using DWCNTs- and Pt-based counter electrodes under 60 mW/cm2 along with statistics

Counter electrode	*J*sc (mAcm−2)	*V*oc (V)	FF	η (%)
DWCNTs	10.75±0.50	0.68±0.01	0.53±0.01	6.05±0.12
Pt	10.73±0.38	0.71±0.01	0.56±0.02	6.80±0.08

obtained spectra were fitted with Z-View software (v2.9c, Scribner Associate, Inc.) in terms of the equivalent circuit shown in the inset of Fig. 3. In general, the EIS spectrum of the DSC containing liquid electrolyte shows three semicircles in the measured frequency from 0.1 Hz to 100 KHz. The ohmic serial resistance (*R*s) in the high-frequency region corresponds to the electrolyte and the FTO resistance, while the resistances *R*ct1, *R*ct2, and *R*diff relate to charge transfer processes occurring at the counter electrode in high-frequency region, at the TiO2/dye/electrolyte interface, and in Nernstian diffusion within the electrolyte in the low frequency range, respectively [31, 32]. The Nyquist plot (Fig. 3a) showed that the value of the *R*s (29.58 Ω cm2) of the DSC fabricated using DWCNTs as counter electrode was a slightly smaller than the *R*s (29.83 Ω cm2) of the Pt-based DSC. *R*s in the high frequency range is mainly due to the sheet resistance of the transparent conductive oxide (TCO) and increases directly proportional to the sheet resistance of TCO [33]. DSCs fabricated with DWCNT and Pt counter electrodes were made by the same type of FTO. Both *R*s values were very close due to the high longitudinal conductivity of DWCNT. However, the value of *R*ct1 of the DWCNTs-based DSC was 12.93 Ω cm2. This value was much larger than that of Pt-based DSC, 3.50 Ω cm2.

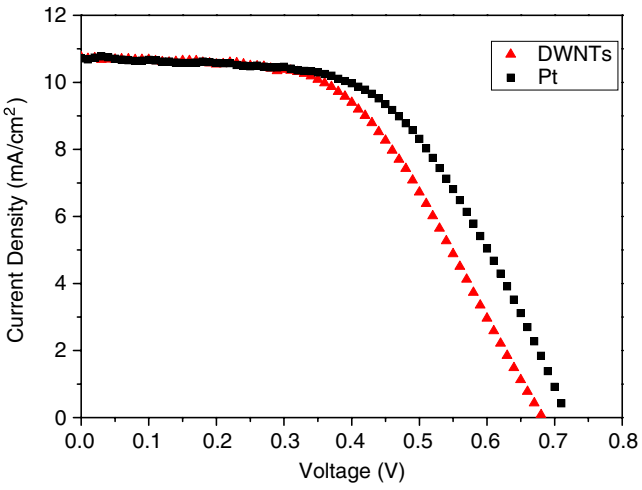

Fig. 2 Photocurrent voltage (*I–V*) characteristics of DSCs fabricated with DWCNTs- and Pt-based counter electrodes

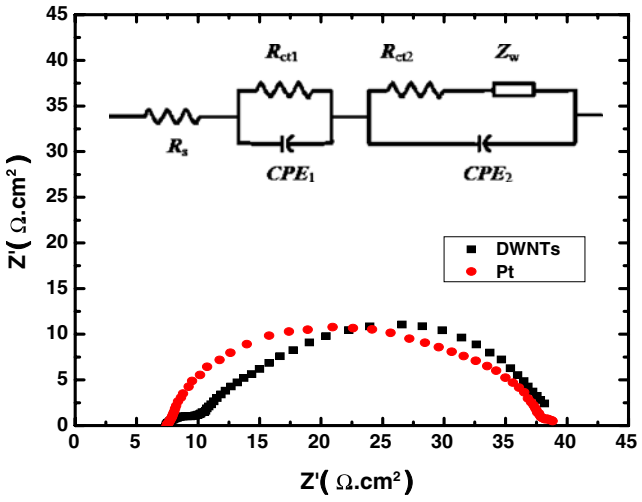

Fig. 3 Impedance spectra of DSCs fabricated with DWCNT- and Pt-based counter electrodes. The *top inset* shows the equivalent circuit

Electrical equivalent circuits have been developed in order to rationalize the charge transfer and transport phenomena that take place in the DSCs [30–32]. However, the interpretation of these phenomena in terms of resistive and capacitive elements is not straightforward due to the complexity inherent to these photo-electrochemical cells. Previous studies have shown that a counter electrode usually affects the performance of cell in three aspects: The first is the electrical property or sheet resistance; the second is the electrochemical property or catalysis efficiency, which is usually determined by the inverse of charge transfer resistance; and the last is the optical property or reflection of illumination [33–35]. The redox reaction resistance *R*ct1 at the counter electrode, the resistance *R*diff of carrier transport by ions in the electrolyte, and resistance R_s due to the sheet resistance of TCO contribute to the internal series resistance of the cell. These resistances bring negative effect on the fill factor and energy conversion efficiency. DSCs fabricated with DWCNT and Pt counter electrodes had quite similar *R*diff or *R*s values because they involved the same electrolyte and FTO. Nevertheless, DWCNT-based DSC showed a higher resistance *R*ct1. The higher value of *R*ct1 led to the higher internal series resistance and resulted in the lower fill factor and the smaller energy conversion efficiency of the DWCNT-based cell shown in Fig. 2 and Table 1. The higher value of *R*ct1 also indicated that the electrochemical property or catalysis efficiency of DWCNT is poorer than that of Pt.

Figure 4 shows the corresponding Bode phase diagrams of the DSCs fabricated with DWCNT and Pt counter electrodes, respectively. Generally Bode phase diagram contains three characteristic frequency peaks, which are assigned in the order of increasing frequency, to Nernst diffusion impedance of the redox species in the electrolyte, diffusion, and recombination of electrons in TiO2 conduction band and charge transfer process at counter electrode/electrolyte interface. From Fig. 4, a strong left shift of the middle-frequency peak (corresponding to the TiO_2/dye/electrolyte interface) is noticed with DWCNTs as counter electrode compared to the case of Pt as counter electrode. This reveals an increase of the electron lifetime in the semiconductor at the same bias voltage in DSC based on DWCNTs [32, 36]. The high-frequency peaks observed in the Bode plots correspond to charge transfer at the counter electrode. There is no significant change in the position of the high-frequency peaks for both DWCNT and Pt counter electrodes studied. The iodide/tri-iodide redox electrolyte is highly corrosive and attacks electrodes. In the case of the DWCNT-based DSCs, the DWCNTs film may be corrupted by the electrolyte, and a small amount of DWCNT particles has a chance to diffuse into the pores of TiO2 network to improve the connectivity between the TiO2 particles, so as to prolong the electron life time in the TiO2 film [37]. As a result, the performance of DSC with DWCNTs as counter electrode was very close to the devices using conventional platinum as the counter electrode, as shown in Table 1 and Fig. 2. The good functionality of DWCNTs as counter-electrode can be attributed to their superior electric conductivity and high electrochemical active surface.

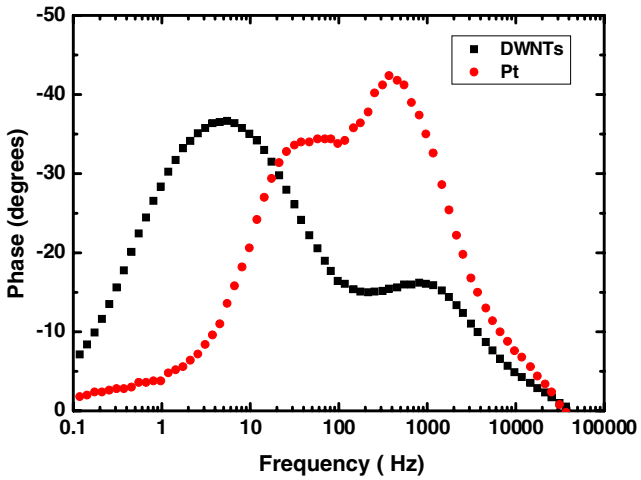

Fig. 4 Bode phase plots of DSCs with DWCNTs- and Pt-based counter electrodes

The efficiency of DWCNT counter-electrode DSC was higher than that of DSCs with SWCNT as counter electrodes reported by Suzuki et al. [10] but lower than that of cells with MWCNTs as counter electrodes reported by Ramasamy et al. [12, 13]. The photovoltaic performance was strongly affected by the specific surface areas of the SWCNT materials [10]. In DSCs, the counter electrode serves to inject charge into the electrolyte and catalyzes the reduction of triiodide:

$$I_3^- + 2e^- \rightleftarrows 3I^-$$

On the other hand, it also has to be well conducting and exhibit a low overvoltage for the reduction of the redox couple in order to carry the photocurrent over the width of each solar cell. Hence, besides the specific surface areas, the adhesion between the counter-electrode layer and the FTO substrate, the work function and electron binding energy of CNTs also exert an influence on the photovoltaic performance. The work function of pure CNTs decreases in the proper sequence of SWCNTs (4.8–5.1 eV), DWCNT (~4.5 eV), and MWCNTs (~4.3 eV) [38–40]. Their electron-binding energy also decreases in the sequence of SWCNT, DWCNT, and MWCNT. Smaller work function and lower electron binding energy may benefit the charge transfer in DSCs. From the data shown in Table 1 and Fig. 2, the performance of DWCNT counter-electrode DSC was poorer than the device using conventional platinum as the counter electrode; however, both kinds of devices demonstrated a very comparable efficiency. Thus, DWCNT had a high electrochemical activity in the iodide/tri-iodide redox reaction.

Conclusions

A low-cost DSC using DWCNT as counter electrode with an energy conversion efficiency of 6.05% has been fabricated. Mesoporous TiO2 films were prepared from the commercial TiO2 nanopowders by screen-printing technique. A metal-free organic dye (indoline dye D102) was used as a sensitizer. DWCNTs were deposited on FTO as counter electrodes. The internal resistance of platinum and DWCNTs counter-electrode-based DSCs were studied by EIS. The DWCNT electrode exhibited a similar DSC performance as the conventional Pt counter electrode. The catalytic activity and cell efficiency of DWCNTs and Pt was investigated and compared. DWCNT has demonstrated a high electrochemical activity in the iodide/tri-iodide redox reaction.

Acknowledgments This work was supported by the National Natural Science Foundation of China (no. 10774046), Shanghai Municipal Science & Technology Committee (nos. 09JC1404600, 0852nm06100, and 08230705400).

References

1. O'Regan B, Grätzel M (1991) Nature 353:737
2. Nazeeruddin MK, Kay A, Rodicio I, Humphry-Baker R, Mueller E, Liska P, Vlachopoulos N, Grätzel M (1993) J Am Chem Soc 115:6382
3. Grätzel M (2001) Nature 414:338
4. Ito S, Chen P, Comte P, Nazeeruddin MK, Liska P, Pechy P, Grätzel M (2007) Prog Photovolt Res Appl 15:603
5. Olsen E, Hagen G, Lindquist SE (2000) Sol Energy Mater Sol Cells 63:267
6. Kay A, Grätzel M (1996) Sol Energy Mater Sol Cells 44:99
7. Lindstrom H, Holmberg A, Magnusson E, Lindquist SE, Malmqvist L, Hagfeld A (2001) Nano Lett 1:97
8. Imoto K, Takatashi K, Yamaguchi T, Komura T, Nakamura J, Murata K (2003) Sol Energy Mater Sol Cells 79:459
9. Lee WJ, Ramasamy E, Lee DY, Song JS (2008) Sol Energy Mater Sol Cells 92:814
10. Suzuki K, Yamamoto M, Kumagai M, Yanagida S (2003) Chem Lett 32:28
11. Lee K, Hwang SH, Moon JH, Noh KS, Lee DY, Kim DH, Sohn KY, Jeon MH (2007) Technical digest of the International PVSEC-17, Fukuoka, Japan, 6P-P6-11
12. Ramasamy E, Lee WJ, Lee DY, Song JS (2008) Electrochem Commun 10:1087
13. Lee WJ, Ramasamy E, Lee DY, Song JS (2009) Appl Mater Interfaces 1:1145
14. Saito R, Matsuo R, Kimura T, Dresselhaus G, Dresselhaus MS (2001) Chem Phys Lett 348:187
15. Shan B, Cho K (2006) Phys Rev B 73:R081401
16. Somani SP, Somani PR, Umeno M, Flahaut E (2006) Appl Phys Lett 89:223505
17. Colomer JF, Henrard L, Launois P, Tendeloo GV, Lucas AA, Lambin P (2004) Chem Commun 22:2592
18. Sugai T, Yoshida H, Shimada T, Okazaki T, Shinohara H (2003) Nano Lett 3:769
19. Sun Z, Huang SM, Lu YF, Chen JS, Li YJ (2001) Appl Phys Lett 78:2009
20. Guo PS, Sun Z, Huang SM (2005) J Appl Phys 98:074906
21. Wang XZ, Li MG, Chen YW, Cheng RM, Huang SM, Pan LK, Sun Z (2006) Appl Phys Lett 89:053127
22. Li HB, Gao Y, Pan LK, Zhang YP, Chen YW, Sun Z (2008) Water Res 42:4923
23. Pappas N, Grätzel M (1999) Process for manufacturing an electrode for an electrochemical device. Polytechnique Federale Lausanne DE. EP0852804
24. Schmidt-Mende L, Bach U, Humphry-Baker R, Horiuchi T, Miura H, Ito S, Uchida S, Grätzel M (2005) Adv Mater 17:813
25. Li XD, Zhang DW, Sun Z, Chen YW, Huang SM (2009) Microelectronics J 40:108
26. Ross MJ, William KR (1987) Impedance spectroscopy: emphasizing solid materials and systems. Wiley, New York
27. Grätzel M (2005) Inorg Chem 44:6841
28. Sakane H, Mitsui T, Tanida H, Watanabe I (2001) J Synchrotron Radiat 8:674
29. Fang XM, Ma TL, Guan GQ, Akiyama M, Kida T, Abe E (2004) J Electro-analytical Chem 570:257
30. Bisquert J (2002) J Phys Chem B 106:325
31. Fillinger A, Soltz D, Parkinson BA (2002) J Electrochem Soc 149:A1146
32. Wang Q, Moser J, Grätzel M (2005) J Phys Chem B 109:14945
33. Han L, Koide N, Chiba Y, Mitate T (2004) Appl Phys Lett 84:2433
34. Hauch A, Georg A (2001) Electrochimica Acta 46:3457
35. Han L, Koide N, Islam A, Chiba Y (2006) J Photochem Photobiol A: Chem 182:296
36. Kuang D, Klein C, Ito S, Moser J, Baker R, Evans N, Duriaux F, Grätzel C, Zakeeruddin S, Grätzel M (2007) Adv Mater 19:1133
37. Lee KM, Hu CW, Chen HW, Ho KC (2008) Sol Energy Mater Sol Cells 92:1628
38. Suzuki S, Bower C, Watanabe Y, Zhou O (2000) Appl Phys Lett 76:4007
39. Liu C, Kim KS, Baek J, Cho Y, Han S, Kim SW, Min N-K, Choi Y, Kim JU, Lee CJ (2009) Carbon 47:1158
40. Ago H, Kugler T, Cacialli F, Salaneck WR, Shaffer MSP, Windle AH, Friend RH (1999) J Phys Chem B 103:8116